# Structural Analysis of the Redesigned Ice/Frost Ramp Bracket

D. R. Phillips[*], D. S. Dawicke[†], S. J. Gentz[‡], P. W. Roberts[3], and I. S. Raju[§]
NASA Langley Research Center
Hampton, VA 23681-2199

## Abstract

This paper describes the interim structural analysis of a redesigned Ice/Frost Ramp bracket for the Space Shuttle External Tank (ET). The proposed redesigned bracket consists of mounts for attachment to the ET wall, supports for the electronic/instrument cables and propellant repressurization lines that run along the ET, an upper plate, a lower plate, and complex bolted connections. The eight nominal bolted connections are considered critical in the summarized structural analysis. Each bolted connection contains a bolt, a nut, four washers, and a non-metallic spacer and block that are designed for thermal insulation. A three-dimensional (3D) finite element model of the bracket is developed using solid 10-node tetrahedral elements. The loading provided by the ET Project is used in the analysis. Because of the complexities associated with accurately modeling the bolted connections in the bracket, the analysis is performed using a global/local analysis procedure. The finite element analysis of the bracket identifies one of the eight bolted connections as having high stress concentrations. A local area of the bracket surrounding this bolted connection is extracted from the global model and used as a local model. Within the local model, the various components of the bolted connection are refined, and contact is introduced along the appropriate interfaces determined by the analysts. The deformations from the global model are applied as boundary conditions to the local model. The results from the global/local analysis show that while the stresses in the bolts are well within yield, the spacers fail due to compression. The primary objective of the interim structural analysis is to show concept viability for static thermal testing. The proposed design concept would undergo continued design optimization to address the identified analytical assumptions and concept shortcomings, assuming successful thermal testing.

## I. Introduction

The proximate cause of the Space Shuttle Columbia accident on February 1, 2003 has been traced to foam material released from the external tank (ET) Bipod region that was transported to and impacted the Orbiter wing leading edge [1]. Since then significant effort has been and continues to be focused on mitigating foam debris release and understanding the ramifications when debris impact occurs.

The ET has three main shell structures, as shown in Figure 1. The upper smaller structure is the liquid oxygen ($LO_2$) tank, the larger lower structure is the liquid hydrogen ($LH_2$)

---

[*] Aerospace Engineer, Lockheed Martin Mission Services, Member, AIAA.
[†] Analytical Services and Materials, Inc.
[‡] Principal Engineer, NASA Engineering and Safety Center.
[§] Structures Discipline Expert, NASA Engineering and Safety Center, Fellow, AIAA.

tank, and the connecting structure is the intertank. The ET thermal protection system (TPS) foam is designed to maintain the fuels in a liquid state, to prevent ice and frost from forming on the exterior surface, and to meet re-entry break-up requirements [1]. The TPS foam is sprayed on most of the acreage of the ET using an automated process, and in other smaller areas, such as near flanges, brackets, and ramps, manual-spray and pour processes are used. Historically, foam with a mass greater than an acceptable limit that is liberated from the ET TPS originates from manual-spray and pour processed areas. For example, critical amounts of foam loss have been reported as originating from the $LH_2$ Ice/Frost Ramp (IFR) stations along the ET [2]. To reduce the amount of foam on the IFRs and to mitigate ice formation, a redesign of the $LH_2$ IFR bracket concept is proposed.

This paper describes the interim structural analysis efforts undertaken during the $LH_2$ IFR redesign effort. First, the proposed IFR bracket design concept is discussed. Next, the details of the finite element model developed to perform the structural analyses are presented. A global/local procedure is used and described in detail. Finally, the results are discussed. The IFR bracket is required to sustain the mechanical, aerodynamic, vibratory, and other loads imposed during prelaunch, launch, and ascent. The responses of the various bracket components to the ascent loading conditions are discussed.

## II. Description of the $LH_2$ IFR bracket design concept

The proposed $LH_2$ IFR bracket concept is shown in the middle of Figure 2. For ease of retrofit, the bracket maintains the same system interfaces as the existing design. The components identical to the existing design are the mounting fixtures for the cable tray supporting the electronic/instrument cables running longitudinally along the tank, the attachments to the tank wall, and the $GO_2$ and $GH_2$ propellant repressurization line (pressline) supports. In the proposed design, the cable tray and pressline supports are connected to a large upper plate that is designed to withstand aerodynamic and thermal loads. The upper plate is connected to a lower plate through eight bolted connections (shown in the inset at the bottom of Figure 2). Included in these bolted connections are blocks of non-metallic material that thermally isolate the upper plate from the lower plate. This isolation is achieved through the insulating properties of the material and by the distance through which the plates are separated. The lower plate is connected to the two mounts that are bolted to the ET.

During launch, the IFR brackets are subjected to mechanical and aerodynamic loading. Mechanical forces are exerted on the brackets by the $GO_2$ and $GH_2$ presslines and the cable tray. Aerodynamic loads act on the bracket.

## III. Finite element analysis

Static analyses are performed using the ABAQUS v6.5-4 commercial software [3]. The analyses are carried out on a Linux machine at the NASA Langley Research Center. The Linux machine contains four AMD 64-bit Opteron processors, each 1.2 GHz, and has 24 GB of main memory.

## A. Modeling assumptions

The model configuration CAD file that was provided for fabrication of a prototype for static thermal testing was also used to generate the finite element model for structural analysis. The model configuratino includes all of the major components (cable tray mount, pressline support, etc.) and several bolted connections that hold the various components together. The bolted connections join the following components:

1. Cable tray mount to pressline support,
2. Pressline support to upper plate,
3. Upper plate to lower plate, and
4. Lower plate to ET mounts.

Connections 1, 2, and 4 in the list above are assumed to be rigidly connected and hence are not modeled explicitly. These components are considered non-critical in this analysis activity because they are unchanged in the redesign. To simplify the finite element model, the non-critical components are joined by a multipoint constraint that allows no relative motion between the connected surfaces (tie constraint).

In the current analysis, Connection 3 is assumed to be structurally critical; failure of the bracket may occur at one or more of the bolted connections that hold the upper and lower plates together. Therefore, these connections are explicitly modeled in the finite element model. A cross-sectional detail of the bolted connection is shown in the Figure 2 inset. The complete assembly of each bolted connection includes a 0.25 in. diameter bolt, a nut, two metallic washers, two thermal washers, a thermal spacer, and a thermal block. The bolt preload, the pitch diameter, and the associated stress concentration are not considered in this interim analysis. The intent of the current analysis is to show viability of the redesign concept for static thermal testing.

## B. Development of the finite element model

The finite element model is constructed using ABAQUS/CAE. A global mesh seed (edge length) of 0.25 in., equivalent to the upper and lower plate thickness, is assigned to the entire model. The configuration is then modeled with C3D10M solid, quadratic tetrahedral elements available in ABAQUS.

### 1. Contact

As shown in the Figure 2 inset, each of the eight bolted connections that hold the upper and lower plates together is composed of eight individual parts. To explicitly model each connection, the individual parts should be included, and interactions between and among the individual parts should be modeled. There are 19 surface-to-surface interactions to consider at each bolted connection. Modeling of such complicated structural assemblage is not a trivial task.

In a single bolted connection, the nut and bolt are the only two components that physically interlock and whose motions are constrained together. Because the bolt preload is not considered in this interim analysis, the washers "float" within the assembly. In addition, the thermal block and spacer are included to thermally isolate the upper plate from the lower plate. These thermal components also float within the assembly. In the connection, each of these floating components comes into contact with the various other components in the assembly. From an analysis point of view, the bolts are the critical components, and the washers can be viewed to have no structural contribution. However, for the plates to remain thermally isolated, the block and spacer cannot experience loads in excess of their structural limit. To realistically model the interactions between the block and spacer with the other components, contact should be used.

For every contact interaction, both a slave and a master surface are defined. As the names imply, the motion of the slave surface depends on the motion of the master surface. Modeling contact and its implementation within ABAQUS require adhering to appropriate rules of thumb [4]. First, the slave surface mesh should be finer than that of the master surface. Second, the slave surface is usually assigned as the surface with the softer material. Third, the analyst must take care to ensure that the mesh is sufficiently refined to calculate the correct deformations. Refining the finite element model to accommodate these rules increases the problem size and computational requirements.

Modeling contact in finite element analyses is not an easy task [5, 6]. When contact is present, the stiffness and load matrices depend on the deformations, and hence the problem is nonlinear. An iteration is performed for a possible solution, after which a residual is computed and the displacements are updated. Iterations are continued until an error norm between successive iterations converges to within a user-specified tolerance.

The use of contact increases the size of the problem being solved because constraint equations for the nodal contact pairs are inserted into the global system of equations. As surfaces come into contact, they may penetrate each other during an iteration. In the next iteration, constraints must be imposed to prevent this penetration; forces are applied to push the surfaces back apart, and the solver iterates until the distance between the two surfaces is nearly zero. "Chattering" may occur as the solution toggles back and forth between penetration and opening of an interface. In addition, large and sudden stiffness changes occur when contact is made, and such abrupt changes can result in convergence difficulties.

The computational effort required to accommodate nonlinear solver iterations increases significantly as more contact interactions are included in the model. For the IFR bracket concept with eight bolts, the complex contact scenario described above occurs eight times. Modeling contact in each of the eight bolted connections is possible, but the convergence of the solution of a problem of this complexity is not guaranteed. As such, a simpler approach to contact is pursued here. As will be discussed later, contact interactions between and among the various components in a single bolted connection are

systematically excluded and inserted to determine their effects on the response of the structurally critical components.

## C. Global/local analysis procedure

### 1. Global model

The global model is first used to determine which of the eight bolted connections experiences the highest stresses under the provided loading conditions. Two configurations, Global Models A and B, of the bolted connections are considered for use in the global model and are shown in Figure 3. Both configurations are highly simplified from the actual design (see Figure 2), with all of the washers and nuts ignored in the models. In both configurations, contacting surfaces are connected with tie constraints, as shown in Figure 4, to relax the demand on the solver and to promote rapid convergence. In Global Model A, the bolts, thermal spacers, and thermal blocks are included between the two plates (see Figure 4a). The tie constraints between the blocks and the plates create a load path that redirects the load into the blocks instead of the bolts. Because in the actual configuration the blocks may be in full or partial contact with the plates, these tie constraints over-constrain the model.

To study the response of the bolts when subjected to a maximum amount of load, an extreme case is considered. In Global Model B, the thermal blocks are removed leaving only the bolts and thermal spacers between the two plates (see Figure 4b). The tie constraints between the bolts, spacers, and plates keep the surfaces in relative position to each other, thus avoiding unrealistic deformation fields that could result from excluding the blocks from the analysis. The displacement field produced by the global model is assumed to be represented accurately, except in regions very local to the bolts. This assumption is justified because the area occupied by the eight bolts is negligible in comparison to the area of the upper (or lower) plate. Note that Global Model B is a further simplification to Global Model A and yet captures the salient features of the bracket configuration.

#### a. Boundary conditions

The boundary conditions of the global model are shown in Figure 5. All degrees of freedom on the bottom face of both of the ET mounts are prescribed zero value:

$u_r = u_x = u_r = 0$

#### b. Loading

The applied loads [7] are provided as $F_r$, $F_x$, and $F_t$ components at several bracket locations. From the provided load, the resultant force for each bracket location is computed. The largest resultant is used to normalize all the loads. The normalized loads are presented in Table 1, and the location of the application of these loads is illustrated in Figure 6. The $GO_2$ and $GH_2$ pressline loads are applied at reference points located at the

center of each respective depression in the pressline support. The interior surface of each depression is "connected" to its reference point by a rigid body constraint. This condition forces the deformation of the depression surface to follow that of the reference point. As a result, the curvature of each depression is maintained. The cable tray loads are applied at the center of the cable tray. The moment ($M_x$) in Table 1 is neglected.* The aerodynamic load is distributed as five sets of concentrated forces (see red arrows in Figure 6), and each set is applied at the centroid of the corresponding pressline support web.

Table 1. Normalized applied limit loads for the global model.

| | Forces | | | Moments |
|---|---|---|---|---|
| | $F_r$ | $F_x$ | $F_t$ | $M_x$ |
| $GH_2$ Pressline | 0.287 | 0.032 | 0.145 | 0 |
| $GO_2$ Pressline | 0.221 | 0.032 | 0.118 | 0 |
| Cable Tray | 0.610 | 0.696 | 0.380 | 1.0 |
| Aerodynamic | 0 | 0.338 | 0.089 | 0 |

**c. Material properties**

All materials used in the finite element analyses are assumed to be homogeneous, elastic, isotropic, and temperature independent. The materials used for each of the components are as follows:

- The upper and lower plates, forward and aft ET mounts, pressline support, and bolts are metallic.
- The thermal block, thermal spacer, and cable tray mount are made from a plastic material. The reported moduli for this plastic material are in the range [595, 3630] ksi.
- The metallic washers are made from stainless steel.
- The thermal washers are made from an acetal material.

The properties selected for each of these materials are presented in Table 2.

Table 2. Material properties used for the analysis of the IFR bracket concept.

| **Material** | ***E* (ksi)** | **ν** |
|---|---|---|
| Metallic | 16500 | 0.342 |
| Plastic | 3302 | |
| Stainless Steel | 28000 | 0.25 |
| Acetal material | 494 | |

* Two sets of analyses were performed with the existing bracket design. In the first set, both loads and moments were applied to the bracket. In the second set, the moments were neglected, and only the loads were applied to the bracket. Comparisons between the two analyses showed that the moments have a negligible effect on the deflections and stresses in the bracket.

**d. Global model deformations**

The exaggerated global model deformations are presented in Figure 7 for the current loading in Table 1 (see Figure 6). The load path is through the upper plate, the bolted connections, then the lower plate, and finally to the ET mounts. The deformation of the plates results in a large moment that causes bending in the bolts. A convergence study with mesh refinement is performed to determine if a single element through-the-thickness is adequate to capture the out-of-plane deformations. An analysis model that uses two elements through-the-thickness produces nearly the same results as the single element model. The deformation field does not show significant change. The minimum displacement magnitude differs by 2%, and the maximum displacement magnitude differs by less than 0.1%. These results suggest that models with one element through the plate thickness yield converged solutions for the out-of-plane deformations.

For the applied loading provided in Table 1, the $\sigma_r$ stresses are the largest stresses observed in the bolts. The $\sigma_r$ stresses in the bolts for Global Models A and B are shown in Figure 8. In Global Model A, the results for the stresses in each of the eight bolts are nearly identical (Figure 8a), and hence no single critical bolt location can be identified. However in Global Model B, three bolts, Bolts 2, 3, and 4 (see Figures 3 and 5), show large stress concentrations, as shown in Figure 8b. While Bolts 2, 3, and 4 have nearly the same peak stresses, Bolt 2 is selected for detailed analysis because the high stresses (compare the light blue and orange regions in Bolts 2, 3, and 4 in Figure 8c) extend over a larger region of the bolt.

**2. Local model**

A region around Bolt 2 is isolated and modeled as the local model (see Figure 6). The local model around Bolt 2 is constructed by cutting the upper and lower plates at the global model partition position and extracting the portions of the plates in the area of Bolt 2, as shown in Figure 9. The distance from the bolt hole to the end of the local model is approximately twelve bolt diameters. This distance is sufficient to avoid edge effects [8]. The exterior edge of the lower plate is less than one bolt diameter from the bolt hole. Because of this small distance, the lower plate may be an critical component of the structure.

The plates are partitioned in the area around Bolt 2 (see Figure 6) to achieve a one-to-one correspondence between the local model boundary mesh and the plate mesh in the global model. The displacements at the nodes on the global/local boundary from the global mesh are extracted and prescribed as boundary conditions to the nodes on the boundaries of the local model (see Figure 9). These displacements adequately constrain the model, and hence no additional boundary conditions are applied. The partitioned global model has approximately 2 million degrees of freedom (DOFs).

The mesh in the local model is refined until converged stresses in the bolt, spacer, and around the holes in the plates are obtained. The original and final converged meshes are shown in Figure 10. (The gap between the upper plate and spacer is exaggerated to show

the mesh refinement through-the-thickness of the plate.) The final local model has approximately 700,000 DOFs. All subsequent models are based on this converged model.

As discussed previously, all contacting surfaces in the area of the bolt and spacer are connected with tie constraints, resulting in an unrealistic representation of the bolt. Three types of modeling strategies, Configuration 1, Configuration 2, and Configuration 3, are pursued to refine the representation of the bolted connection at Bolt 2. Each configuration is chosen to relax certain constraining assumptions and thus improve the bolt modeling; each successive model builds upon the previous configuration. Each of the configurations has approximately 820,000 DOFs.

Certain modeling assumptions are common to all three configurations. Of particular importance is that the spacer cannot transmit any of the tensile loads. Therefore, the tie constraints between the spacer and the plates (see Figure 4) must be removed, and a path must be provided to transmit the loads from the plates to the bolt. Consider the configuration shown in Figure 11. The washers and nut are added to the local model purely to provide a load path from the plates to the bolt. This path is created by "chaining" the components together; the upper plate is tied to the thermal washer, which is tied to the metallic washer, which is tied to the nut, which is finally tied to the bolt. A similar chain of components is created for the lower plate. As in the global models, these chains of tie constraints hold the bolt surfaces in relative position to the plates and prevent any unrealistic deformation fields that could result from the neglect of the blocks from the analysis.

**a. Configuration 1**

All contact interactions are ignored in Configuration 1, shown in Figure 12a. This configuration is used to establish if interpenetration of component surfaces occurs. To simplify the model, a tie constraint is established between the bolt shank and the interior surface of the spacer. The remaining areas of the bolt shank may physically contact the interior surfaces of the washers, and the outer surface of the spacer may physically contact the holes in the plates. If a contact interaction is not set up, interpenetration of the components may occur during the analysis. However, due to the difficulties associated with modeling contact, it is desirable to have as few contact interactions as possible. Therefore, the following assumptions are made.

- The metallic washers have large holes, and hence there is substantial clearance between the washers and the bolts. The assumption is that the model will not deform enough to warrant setting up an interaction in the gap between the washer holes and the bolt shank. Therefore, a gap is maintained in the finite element model (see Figure 12a).
- The thermal washers have smaller holes than the metallic washers, so from a strictly geometric point of view, these washers are more likely to interact with the bolt. However, a gap exists between the washers and the bolt in the undeformed state, so

using the same small deformation assumption discussed for the metallic washers, a gap is left between the thermal washer holes and the bolt shank (see Figure 12a).

- The plate holes may interact with the spacer; however, a small gap between the plates and the spacer exists in the undeformed state. Again using the small deformation assumption, a gap is left in the finite element model (see Figure 12a).

As discussed previously, the spacer cannot transmit any tensile load. Therefore, there is no direct load path between the thermal washers and the spacer. In contrast to the situation between the washers and the bolt and the plates and the spacer, no pre-existing gap exists between the spacer and the washers. A contact interaction should be set up at this interface to be physically accurate. However, it would be computationally advantageous to be able to exclude this contact interaction, and contact is not accounted for at this interface (see Figure 12a). Interpenetration of the spacer with the washers may occur in this model.

Examining the $\sigma_r$ stresses in Bolt 2 shows compression on the upstream side and tension on the downstream side, as expected. In addition, inspection of the deformed model shows that the bolt does not penetrate the washers, and the spacer does not penetrate the plates. It is therefore concluded that for the proposed design and current loading conditions, leaving gaps between the washers and the bolt and the plates and the spacer is a valid assumption.

The displacements from the analysis show that the spacer does penetrate the thermal washers. The maximum compressive stress in the spacer is 12.8 ksi. These results will be discussed further in comparison to Configuration 2. The maximum tensile stresses in the bolt and spacer are 116 and 18.4 ksi, respectively. The tensile stress in the spacer is 16% of the tensile stress in the bolt and is not due to direct load transmission from the plates. As the bolt bends, the tie constraint between the bolt and spacer forces the spacer to bend also, thus inducing tensile stress.

**b. Configuration 2**

Configuration 2 is an extension of Configuration 1 and is shown in Figure 12b. This configuration is used to establish if including contact between the spacer and the thermal washers has a significant affect on the results. The model is set up with the same tie constraints and gaps as in Configuration 1. Building up from Configuration 1, contact interactions are set up at the top and bottom of the spacer for each of the spacer/washer interfaces (see Figure 12b). The contact interaction is defined using a finite sliding formulation. "Hard contact" is used to define the normal behavior, and a coefficient of friction of 0.1 is assumed for the tangential behavior. The top and bottom surfaces of the spacer are assigned as the slave surfaces in the respective contact definitions (see Figure 12b inset). To avoid a numerical phenomenon referred to here as "trimming",[†] the inner surface of each washer is included in the contact master surface (see Figure 12b inset).

[†] Trimming can occur during a numerical analysis when a node on a slave surface falls off the edge of the master surface [4]. The node may then approach the master surface from either behind (a physically incorrect behavior) or in front in successive iterations. As the solver attempts to find an equilibrium

In Configuration 2, the spacer does not penetrate the thermal washers as in Configuration 1. The maximum tensile stress in the spacer is 17.0 ksi, which is nearly the same in comparison to Configuration 1 (<10% difference). However, in contrast to Configuration 1, the maximum compressive stress in the spacer is 70.6 ksi, an 82% increase in magnitude. It is therefore concluded that the contact interaction between the spacer and the thermal washers is a first order effect.

**c. Configuration 3**

Configuration 3 is an extension of Configuration 2 and is shown in Figure 12c. The gaps between the inner radii of the washers and the bolt and the gaps between the holes in the plates and the spacer are maintained. The contact interaction between the thermal washers and the spacer is also maintained. The tie constraint between the bolt and the spacer is removed and replaced with a contact interaction (see Figure 12c). In this contact interaction, the bolt shank is the master surface, and the inner surface of the spacer is the slave surface. The results are discussed in detail in the next section.

## IV. Results

Open literature values for the yield stress of the metallic material are between 125 and 170 ksi. The yield stress corresponding to the material properties used in this report is 125 ksi. Reported values for the yield stress of the plastic material fall between 10 and 33 ksi, and are often higher in compression. Here, the yield stress for the plastic material is assumed to be 33 ksi. A component is considered to have failed if the stress at any location in the component is beyond the yield stress of the material.

The values for the maximum tensile and compressive stresses in the plate radial direction for Bolt 2 as computed using models for Configurations 1, 2, and 3 are presented in Table 3. By comparing Configurations 1 and 2, it is seen that including the contact between the spacer and the thermal washers has a reasonable affect on the compressive stresses (34%) in the bolt, but a lesser affect on the tensile stresses (12%). In all cases, the maximum stress experienced by Bolt 2 is less than the yield stress of 125 ksi, and for Configuration 3 is only 67% of the yield stress.

Table 3. Comparison of maximum $\sigma_r$ bolt and spacer stresses (in ksi) for each local model configuration.

| Configuration | Bolt 2 | | Spacer 2 |
|---|---|---|---|
| | Tensile | Compressive | Compressive |
| 1 | 116 | 80.6 | 12.8 |
| 2 | 102 | 53.4 | 70.6 |
| 3 | 83.3 | 46.6 | 61.8 |

position for this node, “chattering” between the two approaches may occur, making it impossible for the solver to converge on a solution. To avoid trimming, contact master surfaces are extended around corners, as in the Figure 12b inset.

For Configuration 3, the stress distribution in the bracket radial direction for Bolt 2 is shown in Figure 13. Due to the deformations in the plates, the bolt bends about the *t*-axis. This bending causes the bolt to experience compressive straining on the upstream side and tensile straining on the downstream side. For Bolt 2, $\sigma_r$ has much larger maximum tensile and compressive stress values than both $\sigma_x$ and $\sigma_t$ and hence is considered the critical component. With the maximum tensile $\sigma_r$ of 83.3 ksi, Bolt 2 is well below yield for the proposed design and current loading conditions. Note that the bolt preload is neglected in the analysis. Inclusion of the preload may increase the stress in Bolt 2 to beyond yield.

The $\sigma_r$ stress distribution in Spacer 2 in the bracket is shown in Figure 14. As with Bolt 2, for Spacer 2, $\sigma_r$ has a much larger maximum compressive stress value than both $\sigma_x$ and $\sigma_t$ and is considered the critical component. This figure shows that considerable portions of the spacer experience stresses greater than the assumed yield stress of 33 ksi, with a maximum compressive stress of 61.8 ksi. Thus, the spacer fails under the loading.

Figure 14 shows portions of Spacer 2 experiencing tensile stress. As in the case where the tie constraint is used (Configurations 1 and 2), these positive values of stress are not due to a direct load path from the plates through the spacer. This tensile stress is induced by the bending of the bolt. The tensile stress on the downstream side of the bolt is transmitted to the spacer through the contact interaction. In comparison to Configurations 1 and 2, the induced tensile stress in the spacer is lower and nearly zero (in comparison to the compressive stress), as expected.

The largest stress the lower plate experiences is 51 ksi and is the $\sigma_x$ stress. This stress appears at the partitioned edge of the plate and dissipates to nearly zero in the vicinity of the hole. Thus the lower plate is not a critical component of the structure, and the small distance from the bolt holes to the edge of the lower plate does not cause failure of the bracket.

The conclusions drawn from the analysis, given the identified assumptions and boundary conditions, can be summarized as follows:

- Stresses in Bolt 2 are well *below* allowable limits.
- Stresses in Spacer 2 are well *above* the assumed strength of the material of the spacers. Thus the spacer fails under the current loading scenario.
- Stresses in the plates are well below the allowable limits.

## V. Discussion

Throughout most of the analyses presented in this report, the thermal blocks are excluded to simplify the problem. In the local models, any bending resistance offered by the blocks is ignored. Thus the stresses in the bolt are higher than what the stresses would be if the blocks were included. These increased stresses are below yield, and the calculated stresses in the bolt provide an upper bound for the proposed design and current loading conditions. The present analysis therefore provides a conservative approximation of the stresses and deformations in the bolt.

The contact stresses between the spacer and blocks are ignored. It is expected that the contact between the spacer and the block will increase the stress in the spacer. However, the current analysis predicts failure of the spacer. Thus, adding the block and any increase in stress because of this addition will not change the conclusion drawn concerning the spacer behavior.

For the bracket redesign presented in this paper, the thermal blocks and spacers carry all of the compressive load generated by the deformation of the plates. This is a stringent requirement for components that were designed to be non-structural. In any subsequent design optimization effort, the size of the blocks would likely be increased to address the compressive failure observed in this interim structural analysis. Additional thermal analyses and testing would then be required to arrive at a final candidate design.

## VI. Limitations of the presented analysis

The primary objective of this interim analysis is to show concept viability of the proposed bracket design for static thermal testing. As such, many simplifying assumptions are used in the analysis. For example, rigidly connecting the bolt and washer stack to the plates precludes the possibility of joint gapping. Also, to fully assess the state of the joint and bolt, bolt preload needs to be included in the analysis. The inclusion of the preload would cause redistribution of the loads in the proposed configuration and could make stress contributions by the thermal blocks more important. Inclusion of the thermal blocks would require additional contact interactions in the analyses.

## VII. Concluding remarks

Foam from the external tank (ET) $LH_2$ Ice/Frost Ramps (IFRs) is a known debris source during Space Shuttle lift-off and ascent. Efforts were made to eliminate this debris source by redesigning the IFRs. The proposed redesign focused on developing a bracket that would be self-insulating without the use of foam, thus minimizing the debris potential from the IFRs. The proposed redesigned bracket included mounts for attachment to the tank wall, supports for the cables and propellant repressurization lines that run along the tank, an upper plate, a lower plate, and eight complex bolted connections. These bolted connections were considered critical in the structural analyses. Each bolted connection contained a metallic bolt and nut, two metallic washers, two thermal washers, and a non-metallic spacer and block that were designed to thermally insulate the upper plate from the lower plate.

A 3D finite element model of the proposed bracket concept was developed using solid 10-noded tetrahedral elements. The aerodynamic loading provided by the ET Project was used in the analysis. Because of the complexities associated with accurately modeling the bolted connections in the bracket, a global/local analysis procedure was used. In this procedure, first, a global model that did not include contact was constructed to evaluate the response of the bracket as a whole to the applied loading conditions. To simplify the model, at each bolted connection, the outer surface of the bolt was rigidly connected to

the inner surface of the spacer, and the spacer was rigidly connected to the plates. That is, all contacting surfaces were modeled as rigidly connected. The displacement field thus produced by the global model was expected to represent the bracket behavior as a whole accurately, except in regions very local to the bolts. Second, the stresses in each of the eight bolts were examined. One bolt was identified as having high stress concentrations, and a region around this bolt was isolated and modeled as the local model. The local model region around the bolt was modeled by a finer mesh than the global model to delineate the stress field accurately. The displacements at the nodes on the global/local boundary from the global mesh were extracted and prescribed as boundary conditions to the nodes on the boundaries of the local model. Third, contact interactions between and among the various components in the local model were systematically included (i.e., progressively included one at a time) to determine their effects on the response of the bolted structure.

Several local model configurations were chosen to relax certain constraining assumptions and thus improve the bolt modeling; each successive local model built upon the previous configuration. By comparing results among the configurations considered, inclusion of specific contact interactions were observed to have a reasonable effect on the compressive stresses in the bolt, and a lesser effect on the tensile stresses. In addition, considerable portions of the spacer experienced compressive stresses that were greater than the assumed yield stress of the spacer material.

## Acknowledgements

This work was sponsored by NASA under contract NAS1-00135 with Lockheed Martin Space Operations (D. R. Phillips) and contract NAS-xxxx with AS&M (D. S. Dawicke).

## References

1. H. W. Gehman, Jr., *et al*., *Columbia Accident Investigation Board Report*, Volume 1, NASA, Washington, DC, August 2003.
2. External Tank In-Flight Anomaly Report 809-8563, "STS-114/ET-121 Investigation Ice Frost Ramp Team Report (Inputs to NASA IFA Investigation Report)," June 2006
3. ABAQUS User's Manual, Version 6.5, 2004.
4. ABAQUS Analysis User's Manual, Version 6.5, Volume V, 2004.
5. R. D. Cook, D. S. Malkus, M. E. Plesha, R. J. Witt, *Concepts and Applications of Finite Element Analysis*, John Wiley & Sons, Inc., 2002.
6. O. C. Zienkiewicz and R. L. Taylor, *The Finite Element Method, Fifth Edition, Volume 2: Solid Mechanics*, Butterworth-Heinemann, 2000.
7. Provided by Harry Nelson at maf.
8. S. P. Timoshenko and J. N. Goodier, *Theory of Elasticity*, McGraw-Hill, 1951.

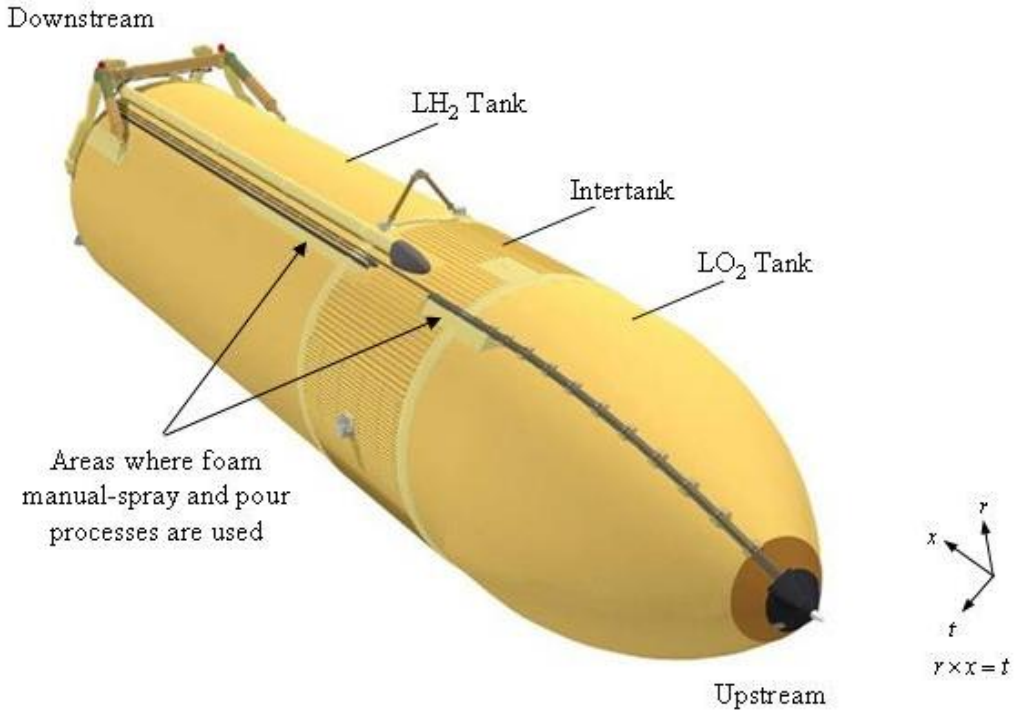


Figure 1: The Space Shuttle External Tank.

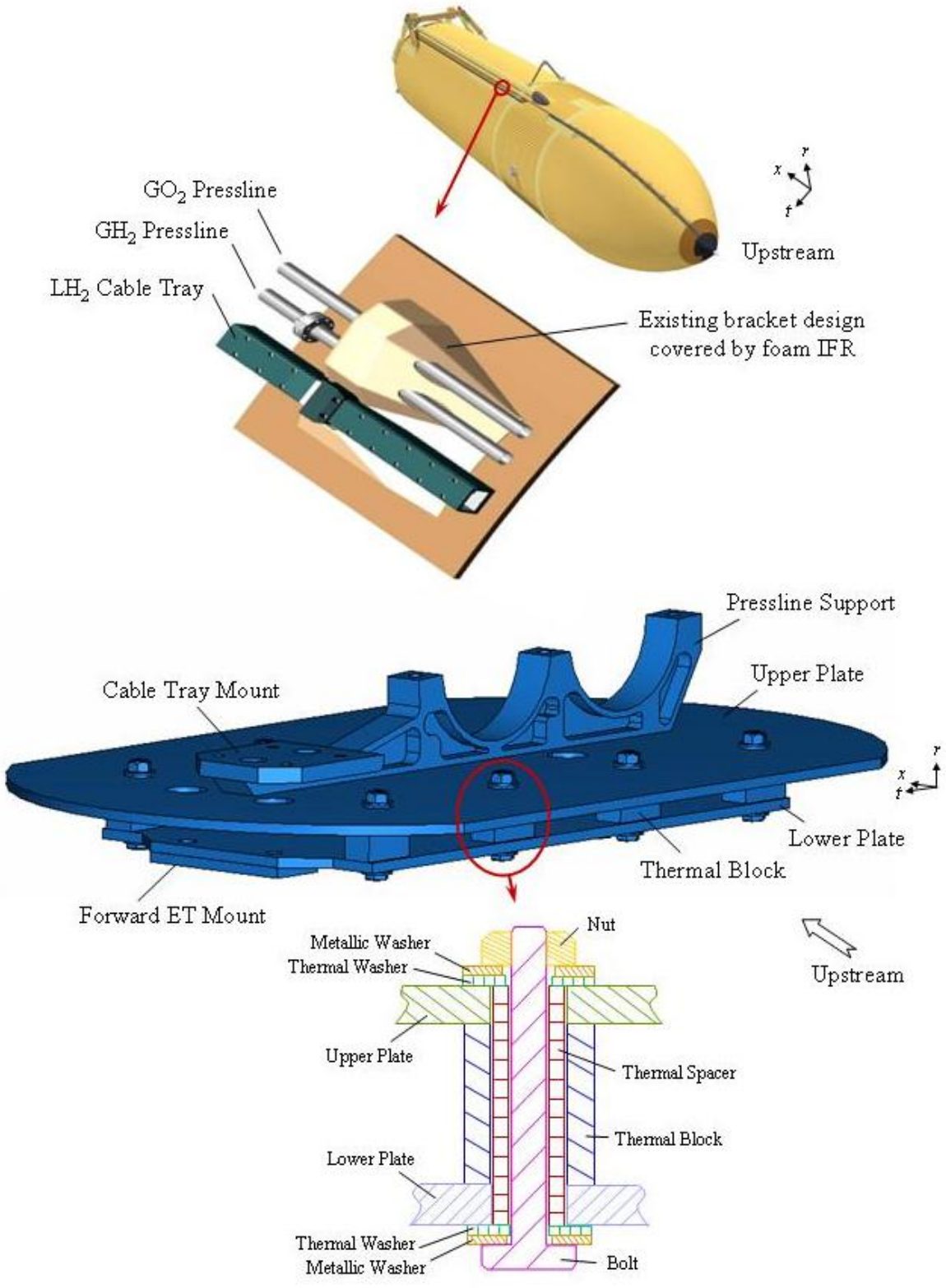


Figure 2: Proposed $LH_2$ IFR bracket design.

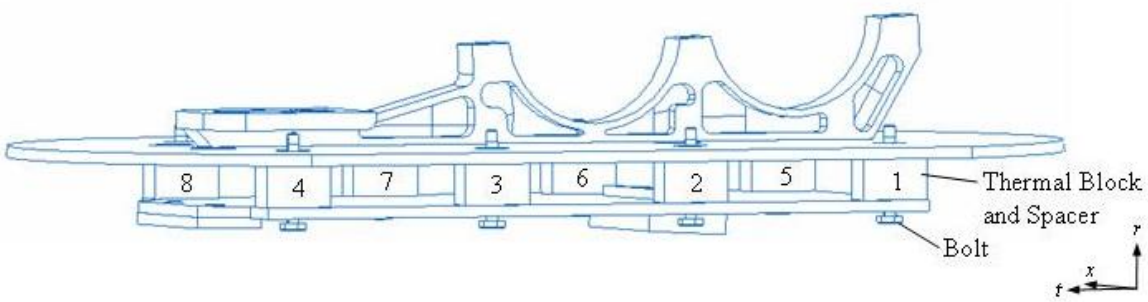


(a) Model A – thermal blocks and spacers modeled (view from Upstream).

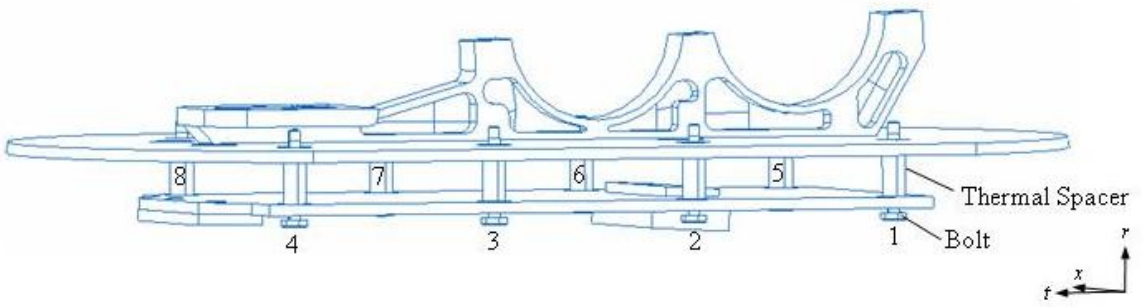


(b) Model B – thermal spacers modeled (view from Upstream).

Figure 3: Two global models considered in the analysis.

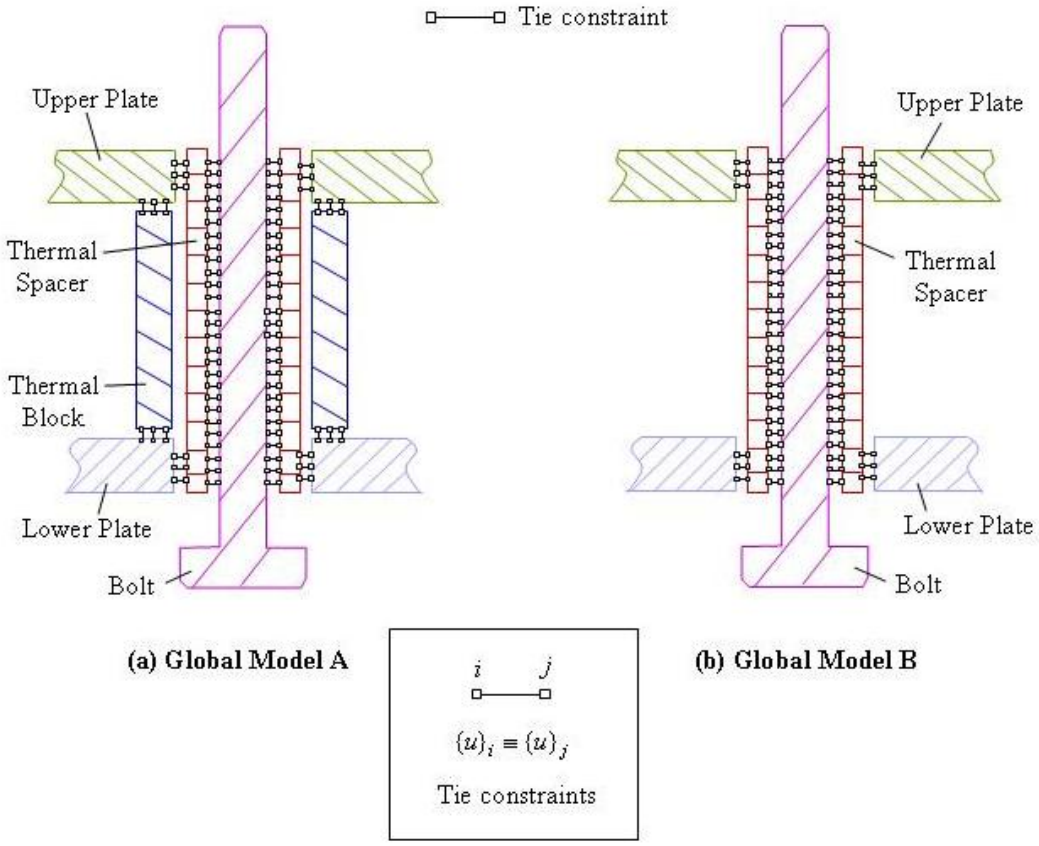


Figure 4: Simplified bolted connection for global analysis.

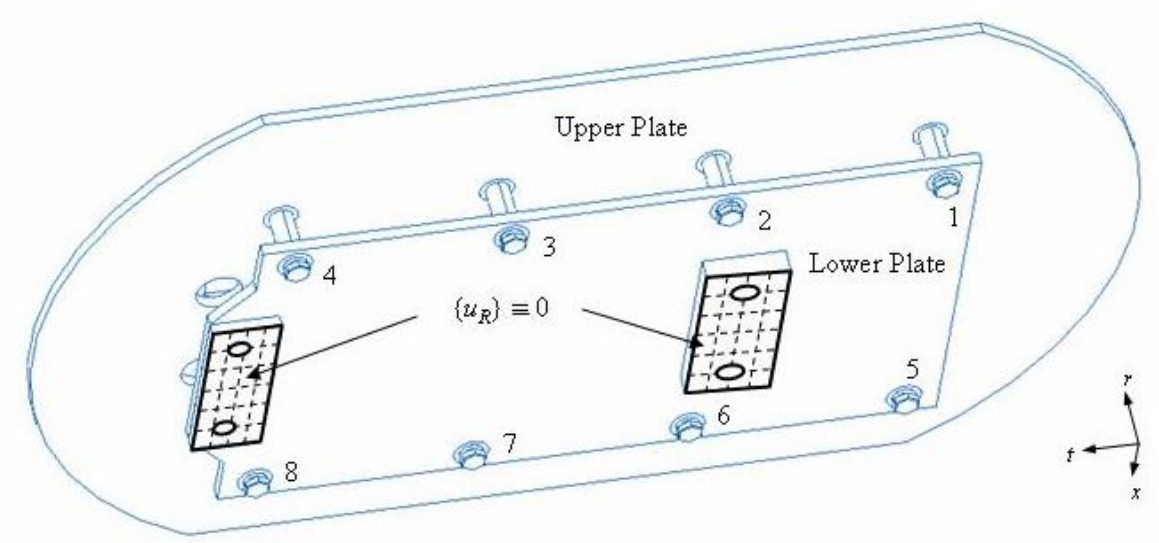


Figure 5: Boundary conditions in the global model.

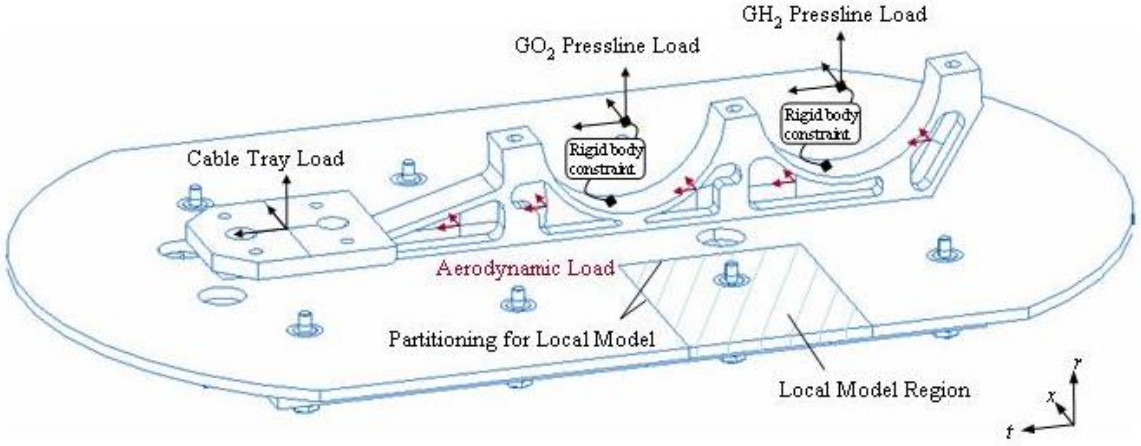


Figure 6: Loading and partitioning of the global model (view from Upstream).

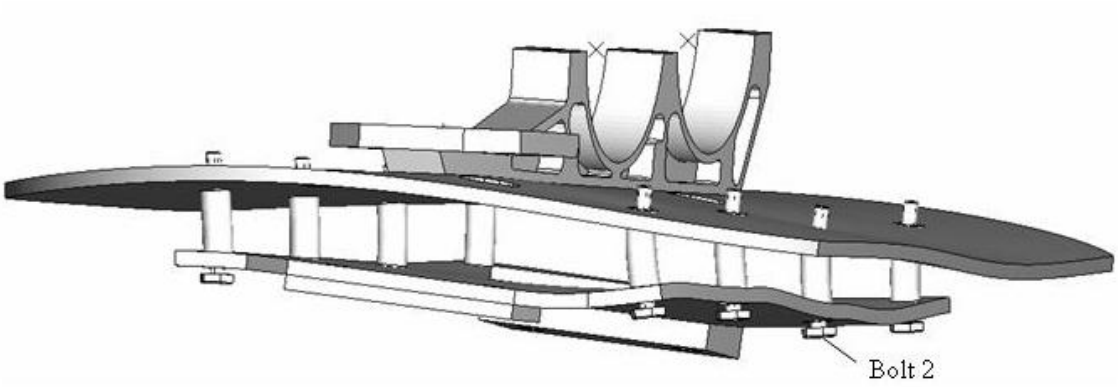


Figure 7: Exaggerated global model deformations.

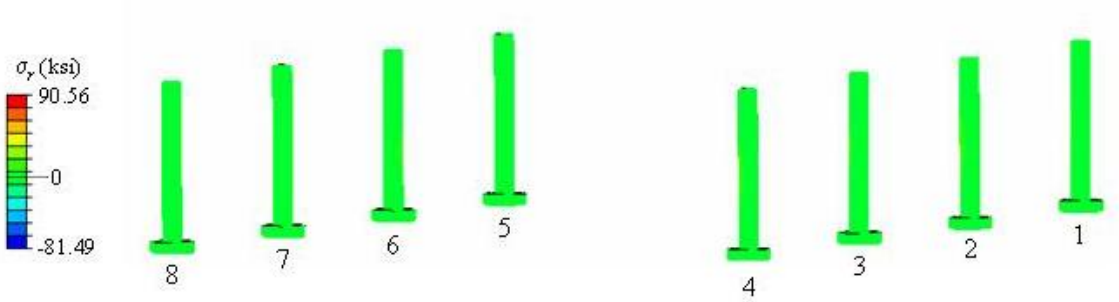


(a) Stresses in the bolts from Global Model A (view from Upstream).

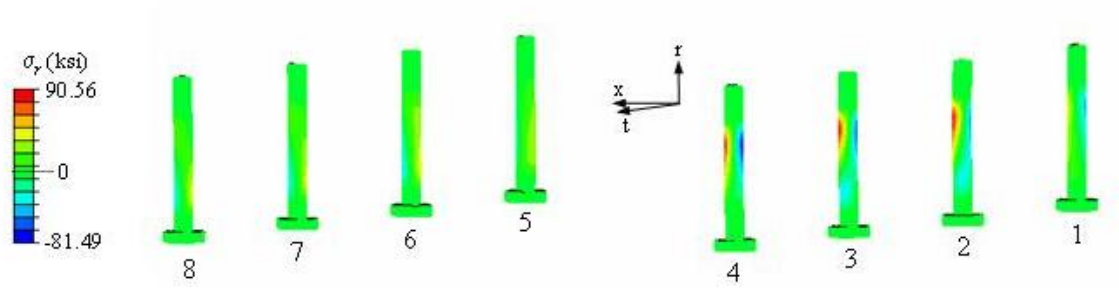


(b) Stresses in the bolts from Global Model B (view from Upstream).

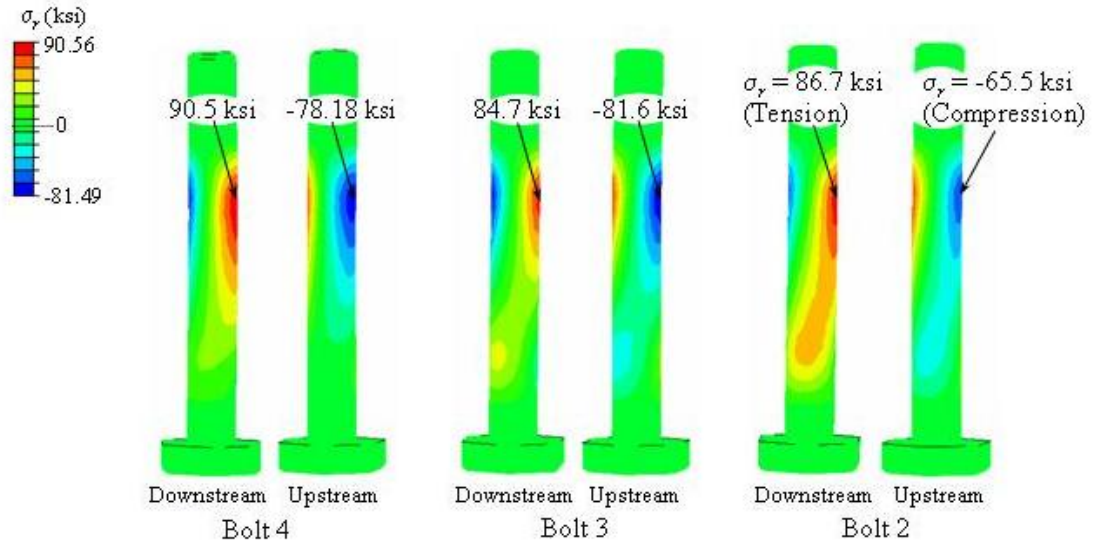


(c) Large stress concentrations in Bolts 2, 3, and 4 from Global Model B.

Figure 8: Stresses in the bolts from Global Models A and B.

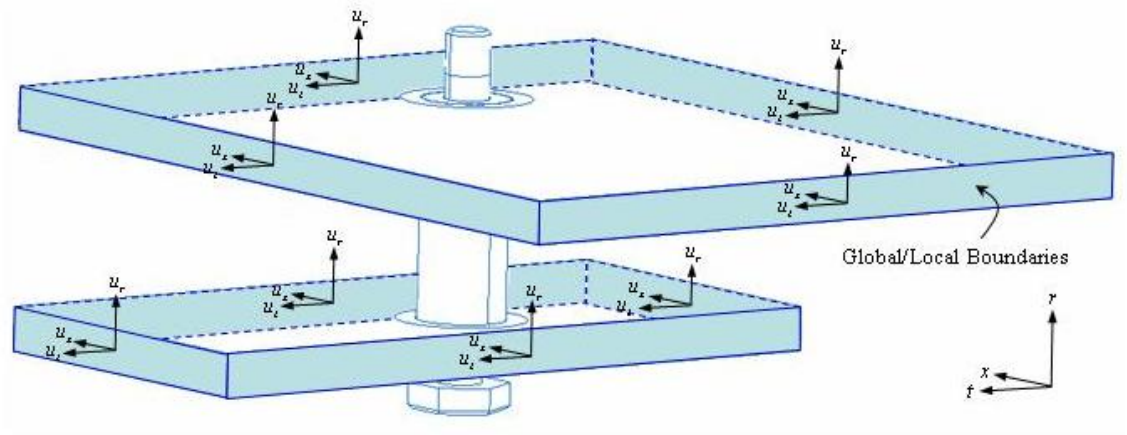


Figure 9: Local model with displacements ($u_x$, $u_t$, $u_r$) from global model prescribed as boundary conditions.

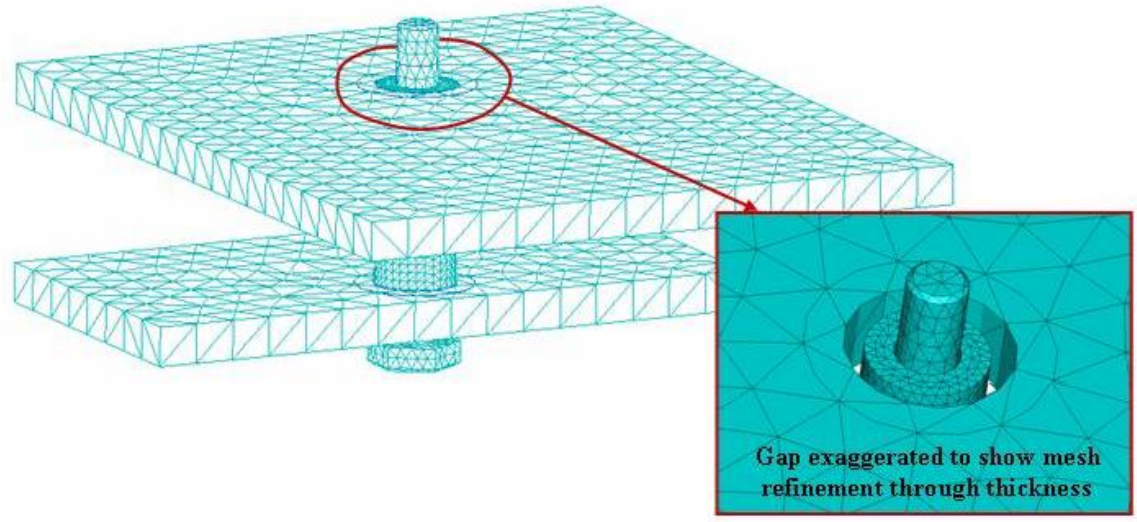


(a) Mesh in partitioned region of global model.

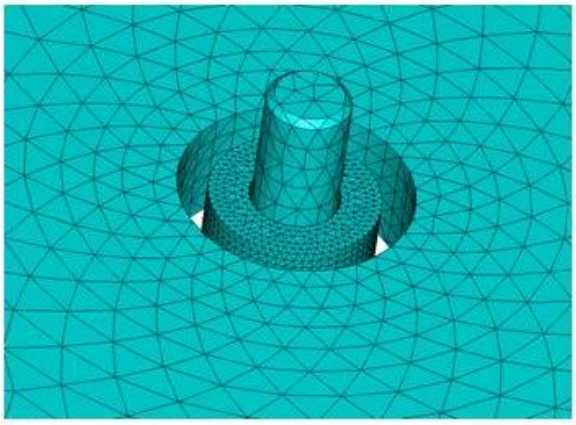

(b) Local model mesh refinement around bolt and spacer.

Figure 10: Original and final converged meshes for the global/local analysis.

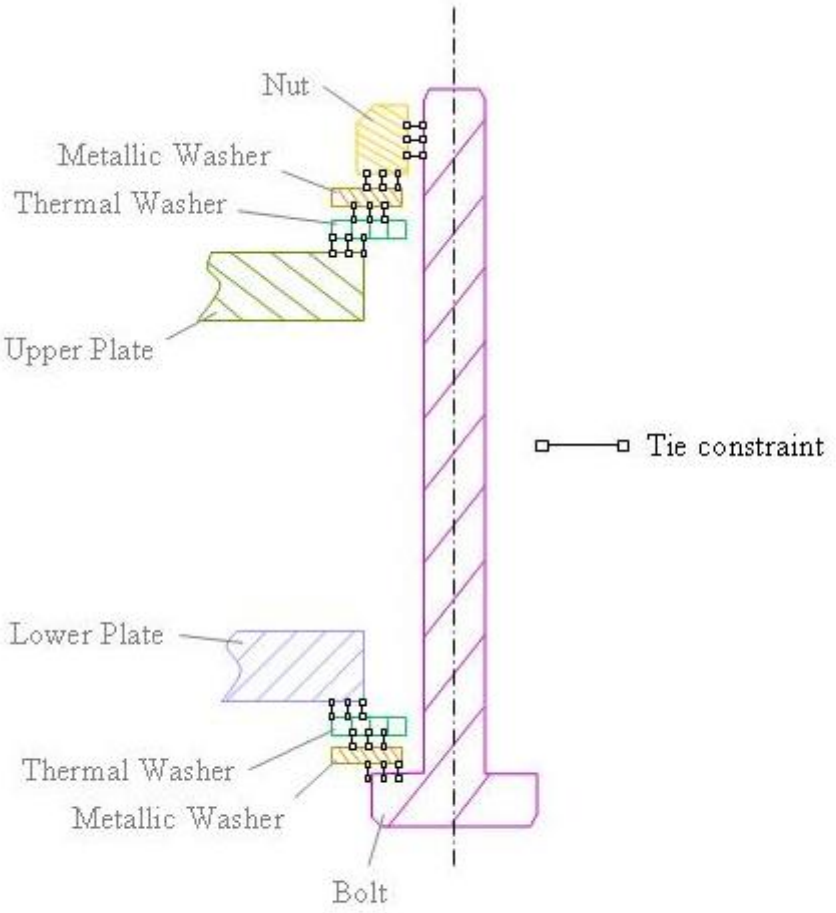


Figure 11: Local model tie constraints to allow load transmission from plates to bolt.

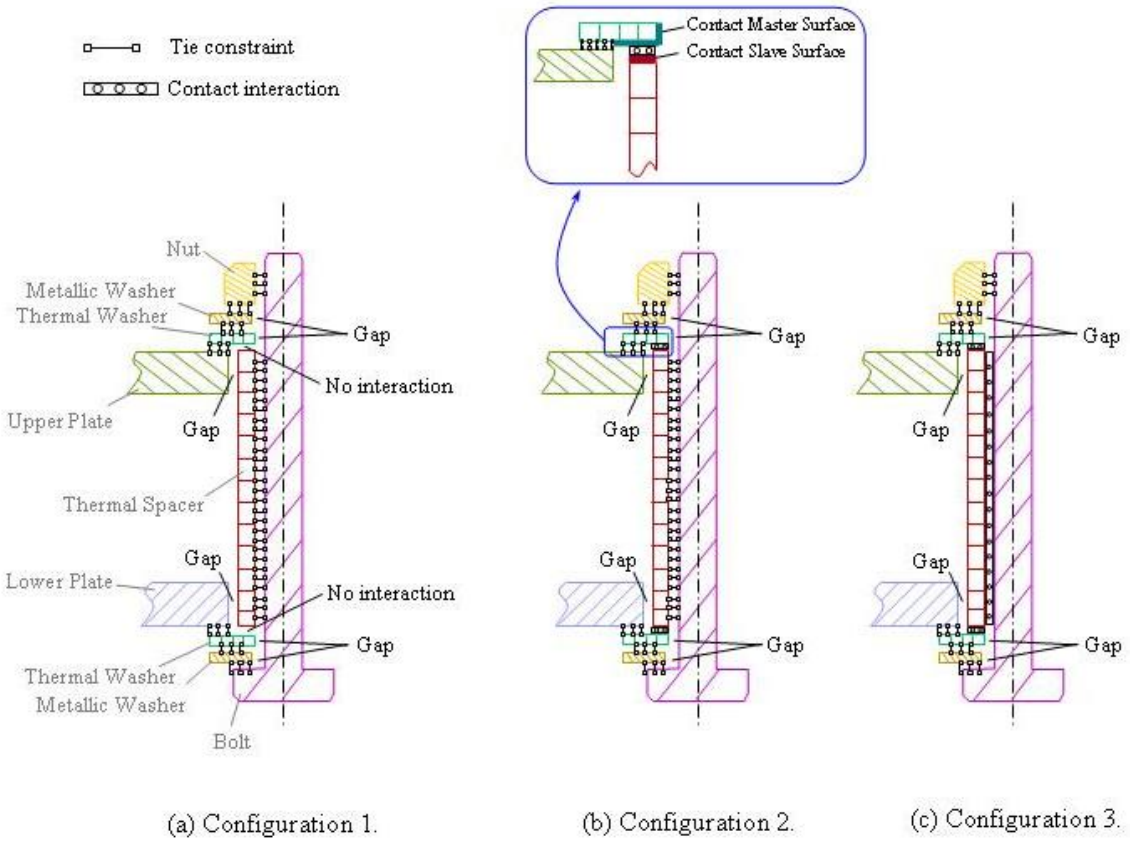


(a) Configuration 1. (b) Configuration 2. (c) Configuration 3.

Figure 12: Local model configurations.

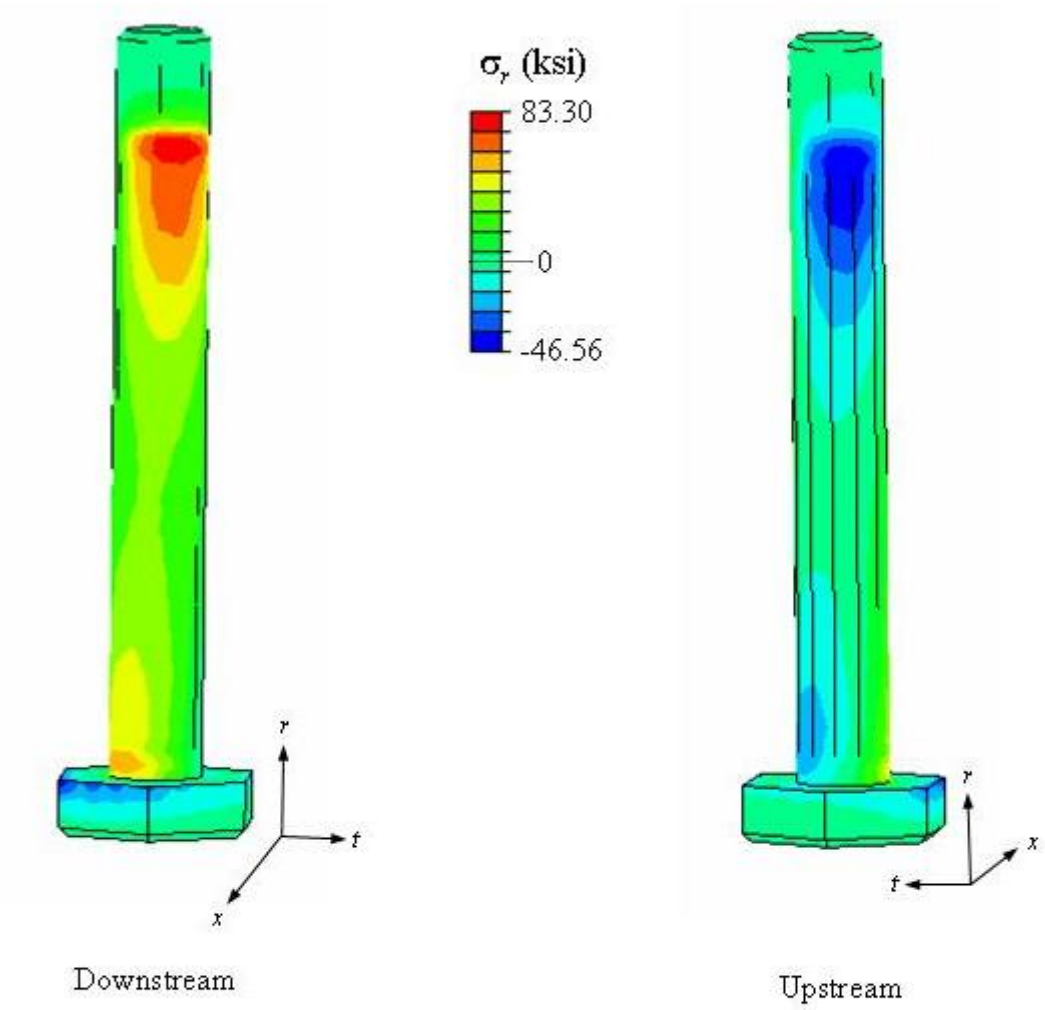


Figure 13: Stress distribution in Bolt 2 from local model Configuration 3.

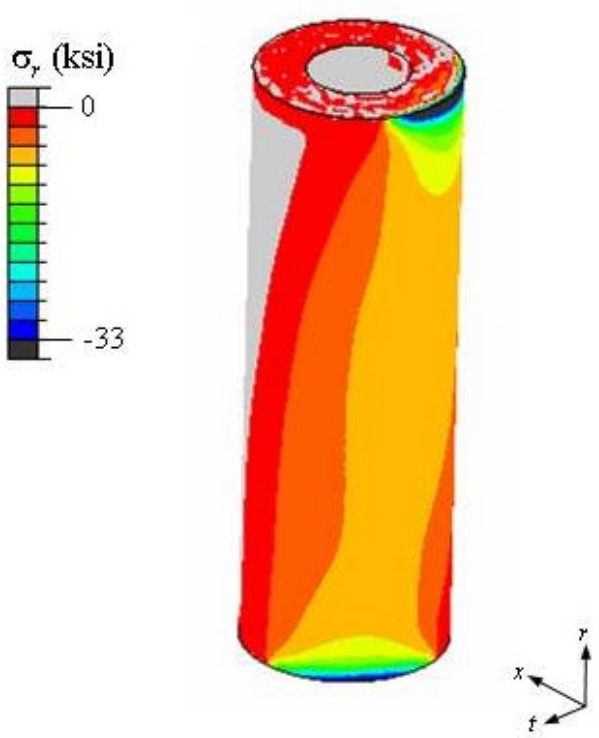


Figure 14: Stress distribution in Spacer 2 from local model Configuration 3.